文章编号：1001－9014(2019)03－0303－07

DOI:10.11972/j.issn.1001－9014.2019.03.008

# Simulation and cold test of a 340 GHz filleted staggered double vane traveling wave tube

SHAO Wei[1], TIAN Han-Wen[1], WANG Zhan-Liang[1], TANG Tao[1], GONG Hua-Rong[1], DUAN Zhao-Yun[1], WEI Yan-Yu[1], FENG Jin-Jun[2], GONG Yu-Bin[1]*

(1. National Key Laboratory of Science and Technology on Vacuum Electronics, University of Electronic Science and Technology of China, Chengdu 610054, China;
2. Beijing Vacuum Electronics Research Institute, Beijing 100015, China)

**Abstract**: Staggered double vane traveling wave tubes have been given a lot of attentions in recent years due to its high power capacity and easy fabrication. However, the loss seriously limits the performance of traveling wave tube with the increasing of frequency, especially in THz wave band. In this paper, a more practical design about staggered double vane structure is proposed with the consideration of the loss and fillets caused by fabrication. The simulation results indicate that the tube with uniform period slow wave structures can obtain over 5 W output power in the frequency range from 320 GHz to 342 GHz. The method of phase-velocity taper is used to enhance the output power and the simulation results show an obvious improvement of the power with more than 28% in the operating wave band. Based on these, the experiment of the fabricated high frequency system with filleted staggered double vane slow wave structure is carried out. The tested $S_{21}$ of pillbox window is above −2.1 dB in the frequency range from 330 GHz to 360 GHz and VSWR (voltage standing wave ratio) is below 1.35 in the frequency range from 334 GHz to 355 GHz. And the tested VSWR of the high frequency system including the pillbox window is below 2 in the frequency range from 335 GHz to 344 GHz, which matches with the simulation results.

**Key words**: filleted staggered double vane, traveling wave tube, loss, fabrication, pillbox window, phase-velocity taper

**PACS**: 84.40.Fe

# 340 GHz 倒圆角交错双栅行波管的仿真与冷测

邵 伟[1], 田瀚文[1], 王战亮[1], 唐 涛[1], 巩华荣[1], 段兆云[1], 魏彦玉[1], 冯进军[2], 宫玉彬[1]*

(1. 电子科技大学 微波电真空器件国家级重点实验室,四川 成都 610054;
2. 真空电子技术研究所,北京 100015)

**摘要**:近些年来交错双栅行波管由于其高功率容量和易加工等优点受到了很多的关注.然而随着器件工作频率的升高,尤其对于太赫兹频段,结构的损耗严重限制了行波管的性能.本文考虑了损耗和加工所导致的圆角等因素,针对交错双栅结构提出了一个更切实际的设计.仿真结果表明,该行波管在320～342 GHz频率范围内能获得大于5 W的输出功率.采用了相速跳变方法来提高输出功率,在整个工作频带内输出功率都得到了大于28%的提升.在此基础上加工了340 GHz交错双栅慢波结构并开展了冷测实验,在330～360 GHz范围内盒型窗的$S_{21}$测试结果大于−2.1 dB且电压驻波比在334～355 GHz范围内小于1.35.同时对包含盒型窗部件的高频系统进行了冷测,其电压驻波比测试结果在335～344 GHz范围内均小于2,且该冷测结果与仿真结果之间趋势基本一致.

**关 键 词**:倒圆角的交错双栅;行波管;损耗;加工;盒型窗;相速跳变

**中图分类号**:TN124　　**文献标识码**:A

**Received date**: 2018-09-23, **revised date**: 2018-11-20　　**收稿日期**:2018-09-23, **修回日期**:2018-11-20

**Foundation items**: Supported by the National Natural Science Foundation of China (61531010)

**Biography**: SHAO Wei (1992-), male, Yunnan, doctoral candidate. Research area involves millimeter wave and terahertz wave vacuum electron devices. E-mail: shaowei12138@qq.com

* **Corresponding author**: E-mail: ybgong@uestc.edu.cn

## Introduction

High frequency and high power are the primary aims for many potential modern applications, including radar systems, security, high-data-rate communications and biomedical imaging[1-2]. The most popular devices applied in these prospects are solid-state devices due to the integration and miniaturization. Although the solid-state devices are broadly used in low frequency, they are difficult to operate within terahertz (THz) wave band. Therefore, the vacuum electron devices (VEDs) with wide bandwidth and high power have attracted a lot of attentions recently[3]. Among the VEDs, traveling wave tubes (TWTs) are one of the most important devices due to the broad bandwidth and high output power[4]. As the core part of TWT, the slow wave structures (SWSs) influence the performance of the TWT to a great extent.

Traditional SWSs include helix, folded waveguide, coupled-cavity and so on. Among these SWSs, folded waveguide is widely used at millimeter wave and terahertz wave band because of its wide bandwidth and high output power. But the circular beam tunnel of this structure makes it difficult to achieve microfabrication processes. In addition, the sizes of the structure are decreased rapidly with the increasing frequency, which will lead to a lower current carrying capacity. Thus, the sheet electron beam has been paid a lot of attentions in recent years. Compared with the circular beam, sheet electron beam has such advantages as a smaller current density and a weaker space-charge density while the focusing of the sheet beam is more difficult, especially for a long-distance stable transportation[5]. Fortunately, the periodic cusped magnetic (PCM) focusing system proposed by John Booske[6] has been proved that can effectively restrain the Diocotron instability of the sheet beam[7]. Furthermore, the experiment reported in Ref. [8] also confirms that PCM system can focus the sheet electron beam with more than 93% beam transmission efficiency in a 112.7 mm slow wave structure. Therefore, the rectangular SWS with a normal sheet beam tunnel has been paid significant attentions due to its high output power and easily to be fabricated.

Staggered double vane structure as one of the rectangular SWS was firstly proposed by Shin et al. with a stable fundamental mode operation[9-13]. In Ref. [10], a 220 GHz half-period-staggered double-vane TWT amplifier was reported, with the simulated output power of 150 W ranging from 210 ~ 260 GHz for the current density of 357 A/cm$^2$. To make a good match between SWS and input/output coupler, a ridge-loaded input and output coupler was proposed by Jianqiang Lai *et al.* [14] and the simulation results show that the TWT can produce over 1 kW of peak power in range from 90 ~ 95 GHz.

However, when the TWT operates with a higher frequency, there are some technical difficulties that may influence the performance of TWT seriously. One of them which needs to be solved urgently is the circuit loss. Circuit loss is one of the most important characteristics of the SWSs, and the loss generally contains conductor loss and insertion loss. For an all-metal staggered double vane SWS at THz wave band, the conductor loss mainly affects the amplification of the input signal. Furthermore, the conductor loss greatly increases with the increasing of the operating frequency due to the aggravated skin effect and the accuracy limitation of fabrication technology. Especially the surface roughness is in the same order as the skin depth in sub-millimeter wave band which leads to increasing of the circuit loss as well. So it is necessary to consider the surface roughness of the SWS and input/output coupler caused by fabrication tolerance.

The fabrication technology also causes the variations of the structure such as fillet and deformation, which will result in the characteristics of the structure changing. The deformation can be avoided by improving the accuracy of the fabrication while the fillet is existed ineluctably. So the modified structure with fillet should be considered in the simulation so that the simulation results can have a well-match with the actual results.

Because the velocity of beam decreases considerably at the end of beam-wave interaction, the synchronous conditions are broken and the interaction cannot be carried on effectively. So the method of phase-velocity taper is applied to resynchronize the wave and beam so that the gain and electron efficiency can be enhanced[15-16].

In this paper, the circuit loss is considered with a corrected conductivity and a 340 GHz filleted staggered double vane TWT is designed as shown in section II. The high-frequency characteristics and beam-wave interaction are presented in section II, III respectively. Based on these, the prototype of the SWS is manufactured and the test results of the transmission characteristics are reported in section IV. Furthermore, a 340 GHz diamond window is designed and is also manufactured and tested. The differences between the simulation results and the test results are illustrated in section IV finally. And some conclusions are drawn in section V.

## 1 High-frequency characteristics of the filleted staggered double vane SWS

The staggered double vane structure has been widely studied in recent years due to its simple geometric construction and wide operating bandwidth. The shift of the lower part of the vane with respect to the upper part is a half period. To decrease the operating beam voltage, the structure operates with the fundamental mode which is under the first spatial harmonic wave regime. Considering the transverse approximate symmetry and simplifying the fabrication, the structure can be fabricated with upper and lower parts separately.

In fact, there is a problem that the grooves will exist a rounded corner in the processing of fabrication by means of the high speed milling method. So the model is modified with the fillet as shown in Fig. 1 and the fillet radius of 0.05 mm, which cannot be neglected, is selected with the actual fabrication technology. This modified SWS can be called filleted staggered double vane slow wave structure.

The performance of the structure is determined

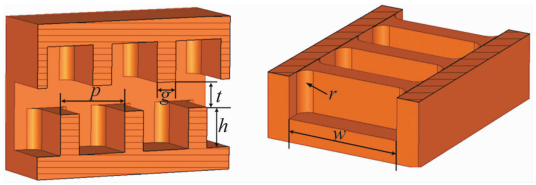


Fig. 1　The section view of metal model of the staggered double vane structure
图 1　交错双栅结构模型的剖视图

greatly by some of the geometry parameters as shown on Table I: the vane height, width, thickness are $h$, $w$, $g$, respectively, the vane period is $p$ and the beam tunnel height is $t$. The dispersion and the interaction impedance[14] are two important parameters that can represent the SWS's circuit characteristics to some extent.

The dispersion curve can be inferred by

$$\frac{v_p}{c}=\frac{\omega}{\beta c}=\frac{2\pi f}{(\varphi/p)c}=\frac{2\pi pf}{c\varphi} \quad , \quad (1)$$

where $p$ is the period length of the structure, $\varphi$ is the phase shift, $\omega$ is the angular frequency, $c$ is the velocity of light and $v_p$ is the phase velocity.

For the slow wave structure of traveling wave tube, the interaction impedance of nth spatial harmonic is defined by

$$K_{cn}=\frac{|E_{zn}|^2}{2\beta_n^2 P} \quad , \quad (2)$$

$$\beta_n=\frac{\varphi}{p} \quad , \quad (3)$$

where $P$ is the transmission power along the axial direction of the structure, $E_{zn}$ and $\beta_n$ is the amplitude of the axial component of the electric field and the phase constant of nth spatial harmonic.

**Table 1　Optimized design dimensions of unit period of the SWS**

**表 1　单周期慢波结构的优化参量**

| Parameters | dimension(mm) |
|---|---|
| $w$ | 0.5 |
| $p$ | 0.31 |
| $g$ | 0.09 |
| $h$ | 0.18 |
| $t$ | 0.12 |
| $r$ | 0.05 |

Fig. 2 shows the dispersion curve and the interaction impedance with/without fillet. As can be seen, the normalized phase velocity of the SWS with fillet is greater than the SWS without fillet at same frequency. The bandwidths and interaction impedance of these two structures are nearly the same.

The combination of the SWS with 165 periods, the input/output coupler and rectangular attenuator comprises the model of the tube, which is shown in Fig. 3. To restrain the signal reflection and the self-oscillation of the structure efficiently, a well-match input/output coupler for this SWS is designed[14] and it includes two components: the input/output connector and transition structure. The transition structure contains five periods and the gradual transition is formed by the linearly decreasing heights of the vanes and the increasing thicknesses when the vanes close to the input/output port.

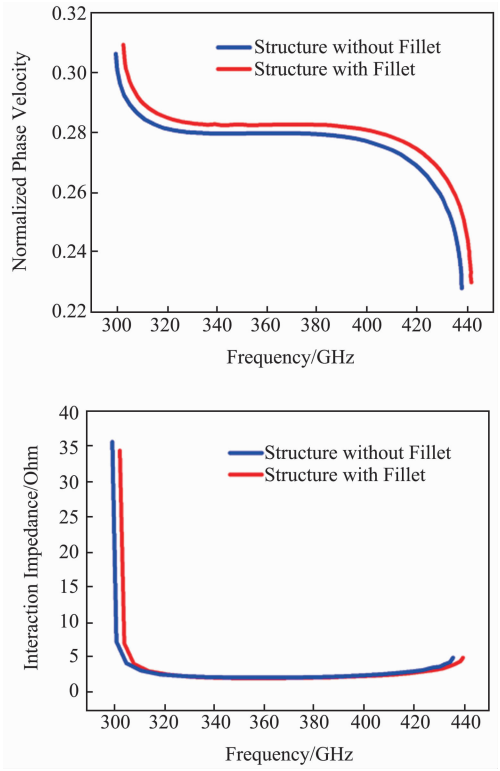


Fig. 2　Dispersion curves and impedance of the structure with/without fillet
图 2　有无倒圆角的结构的色散曲线与耦合阻抗

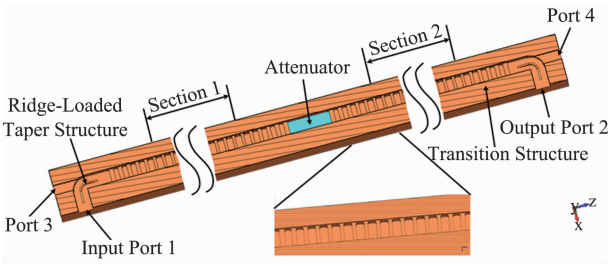


Fig. 3　The section view of the complete tube with ridge-loaded waveguide
图 3　包含脊加载波导的整管剖视图

A rectangular attenuator is also designed to prevent the reflection signal oscillations caused by the impedance mismatch of the structure. The position of the attenuator inserted in the SWS can be inferred from Ref. [17] and the final position is shown in Fig. 3. As can be seen from this figure, the SWS is divided into three sections: a pair of attenuators occupying 5 periods which are embedded in the top and bottom of the structure, the front section (See Section 1) and the rear section (See Section 2) of the SWS contain 45 and 120 periods, respectively. And *CP-BeO* (carburized porous beryllium oxide) is considered for the attenuator with a loss tangent of 0.5 and rel-

ative permittivity of 6.5.

The internal surface of the slow wave structure is always considered as a smooth surface when calculating the loss of metal model in the simulation. However, a tiny fluctuation of the surface will exist in the SWS due to the error of actual fabrication, which is also called the surface roughness. This greatly effects the performance of the SWS with a non-negligible loss, especially in the sub-millimeter or THz wave band. So there is a major error between the simulation results and the actual without the effects of the surface roughness. A corrected conductivity is considered with the surface roughness and the criterion equation can be derived from[18-19]:

$$\sigma_c = \frac{\sigma}{(1+\frac{2}{\pi}\arctan(1.4\times(\frac{R_s}{\delta})^2))^2} \quad , \quad (4)$$

where $\sigma = 5.8\times10^7$ S/m is the original conductivity of the copper, $R_s$ is the surface roughness, and $\delta$ is the skin depth which is given as follows.

$$\delta = \sqrt{\frac{2}{\omega\mu\sigma}} \quad , \quad (5)$$

where $\mu$ is the permeability of vacuum and $\omega$ is the angular frequency.

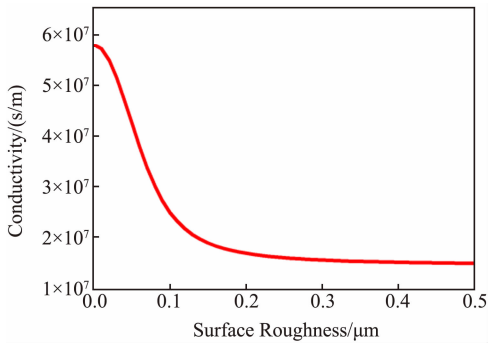


Fig. 4 The corrected conductivity versus different surface roughness at 340 GHz

图4 340 GHz处对应不同表面粗糙度的修正电导率变化曲线

Fig. 4 shows the conductivity versus different surface roughness at the same frequency of 340 GHz. The surface roughness of the oxygen-free copper machined by the high-speed milling method can achieve 0.2 μm. It can be observed that the conductivity is converging to a definite value along with the increase of surface roughness. Here, $\sigma_c = 1.45\times10^7$ S/m is applied in this paper finally with the consideration of some unpredictable flaws in the fabrication process.

The transmission characteristics of the structure with/without fillets are shown in Fig. 5. It is obvious that the high frequency system with the attenuator has a low reflection. And the results with/without fillets have few differences as seen from the figure. The reflection coefficient ($S_{11}$) with attenuator keeps below −20 dB in the frequency ranging from 330 GHz to 350 GHz and the curves of $S_{31}$ and $S_{41}$ also show that the signal is cutoff at the beam tunnel ports to the electron gun and to the collector.

Considered that the region of beam-wave interaction

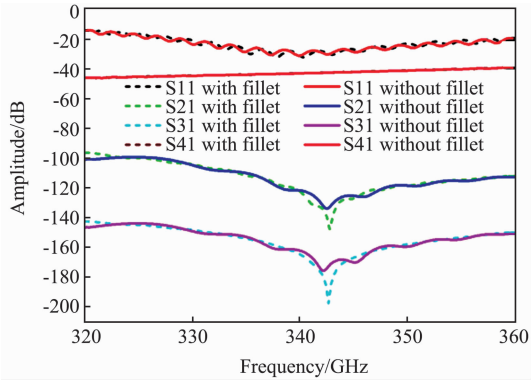


Fig. 5 The transmission characteristics of the structure with attenuator

图5 考虑衰减器的结构传输特性曲线

in the tube requires a vacuum and airtight environment, a pillbox window is used to separate the air from input and output ports as shown in Fig. 6. The dimensions of the window are given in Table II: the radiuses of the circular waveguide and window are $R_1$ and $R_2$, respectively. Corresponding thickness of them are $d_1$ and $d_2$. And $a_0$ and $b_0$ are the width and height of the standard waveguide. The transition waveguide is used to connect the standard waveguide and the input/output port of the tube and diamond is selected as the material of the window.

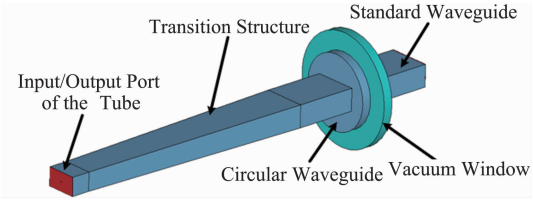


Fig. 6 Three-dimensional vacuum model of the pillbox window

图6 盒型窗的三维真空模型示意图

**Table 2 Design dimension of the pillbox window**

**表2 盒型窗的尺寸参数**

| Parameters | Dimension (mm) |
|---|---|
| $R_1$ | 0.6 |
| $R_2$ | 0.9 |
| $d_1$ | 0.15 |
| $d_2$ | 0.15 |
| $a_0$ | 0.71 |
| $b_0$ | 0.36 |

Fig. 7 gives the transmission characteristics of the pillbox window with the corrected conductivity. The results indicate that the reflection coefficient $S_{11}$ is below −25 dB and $S_{21}$ is about −0.8 dB in the frequency range from 320 GHz to 360 GHz. The transmission characteristics of the whole tube including the pillbox window are shown in Fig. 8 and it illustrates that the window affects the performance of the structure to some extent

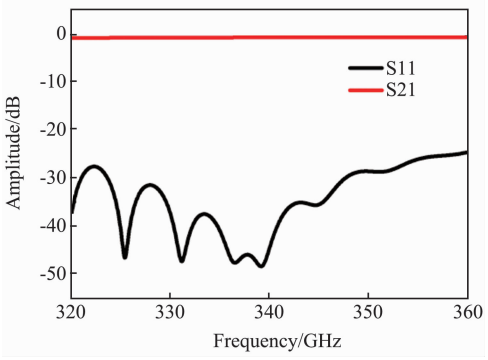


Fig. 7　S-parameters of the pillbox window
图 7　盒型窗的 S 参数曲线

which leads to worse reflection characteristics.

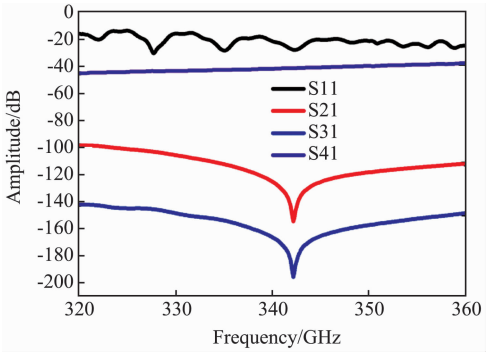


Fig. 8　The transmission characteristics of the tube with pillbox window
图 8　包含盒型窗的整管传输特性曲线

## 2　Beam-wave interaction

The particle-in-cell (PIC) simulation[20] is carried out in this section and a sinusoidal signal with 10 mW average power is selected as the input source of the tube. The beam-emitting source with 22.1 kV beam voltage and 43 mA beam current (current density 200 A/cm$^2$) is applied and a uniform longitudinal magnetic field of 0.6 T is used to focus the beam. The conductivity of the metal walls is defined as mentioned previously.

Figure 9 shows the input and output signals with conductive loss at 340 GHz. A stable output signal can be obtained after 1.8 ns interaction time with 5.7 W output power and 27.6 dB gain. The spectrum of the output signal is shown in Fig. 10, which can be seen that the spectrum is quite pure and there are no high order harmonics.

The results of average output power versus discrete frequency points sweeping from 320 to 348 GHz are given in Fig. 11 and the instantaneous bandwidth of 22 GHz in the frequency range from 320 to 342 GHz is achieved with over 5 W output power. And the maximum output power reaches 12.8 W at 328 GHz, which corresponds to 31.1 dB gain and 1.3% RF efficiency.

The output power drops in the lower and upper cut-off frequency due to the beam-wave synchronous condition is not well-satisfied as well as the signal reflections from input and output ports.

The method of phase-velocity-taper can be utilized to improve the performance of the TWT which is largely damaged by the loss. The tapering method proposed by Ref. [15-16] is applied in this structure and the tapering period length of 0.308 mm is optimized to begin from

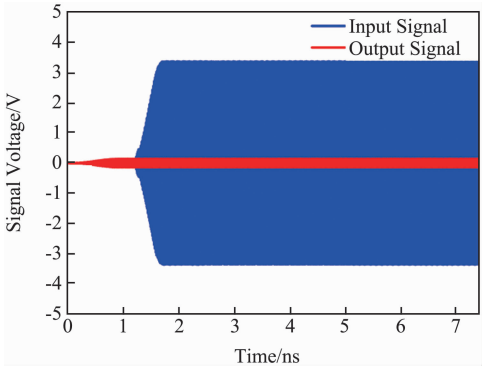


Fig. 9　Input and output signal of the structure at 340 GHz
图 9　340 GHz 处的结构输入输出信号图

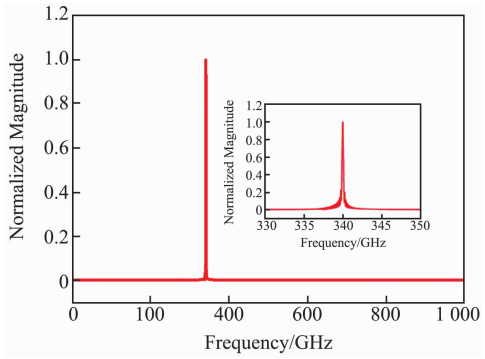


Fig. 10　The spectrum of the output signal at 340 GHz
图 10　340 GHz 处的输出信号频谱图

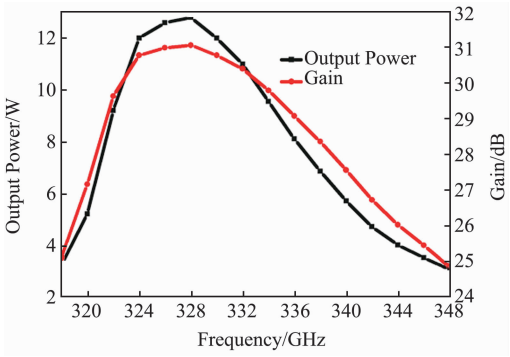


Fig. 11　The results of the average output power and gain versus frequency
图 11　平均输出功率及增益随频率变化的结果

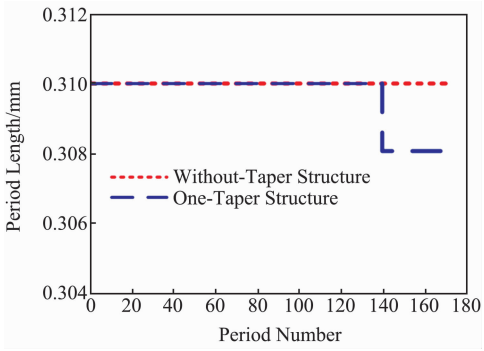


Fig. 12 The description of tapering period length and number of the structure
图 12 相速跳变结构的跳变周期长度以及数量的示意图

the 90th period to the end of the section 2, which are shown in Fig. 12.

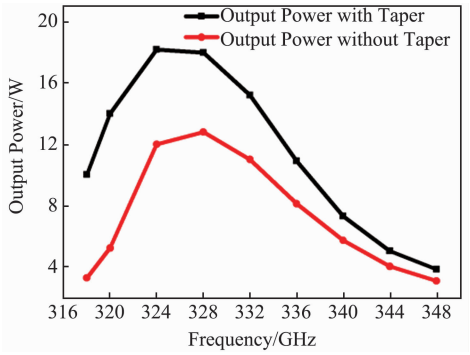


Fig. 13 The output power versus different frequency compared with the result without taper
图 13 有无相速跳变的输出功率随频率的变化曲线

The average output power versus different frequencies is shown in Fig. 13 and the result shows that the output power gets a great improvement within a wide bandwidth by tapering the phase-velocity of the circuit.

## 3 Cold test of the high frequency system

Based on the above theoretical design and simulation, a 340 GHz sheet beam filleted staggered double vane high frequency system has been fabricated by high-speed milling and EDM (electrical discharge machining) successfully, which is shown in Fig. 14.

The manufactured structure consists of attenuator, SWS, ridge-loaded input/output waveguides and pillbox window. It can be observed from Fig. 14 that the fabricated SWS not only can well manifest the features of the vanes by microscope but also reveals the tough irregular surface of the vane.

The pillbox window is tested firstly as shown in Fig. 15 and the tested result shows that the VSWR is below 1.35 in the frequency range from 334 GHz to 355 GHz while this is not in accord with the simulation result. The main reason for the difference between these two results is the influence caused by the quality of welding and assembly of the pillbox windows.

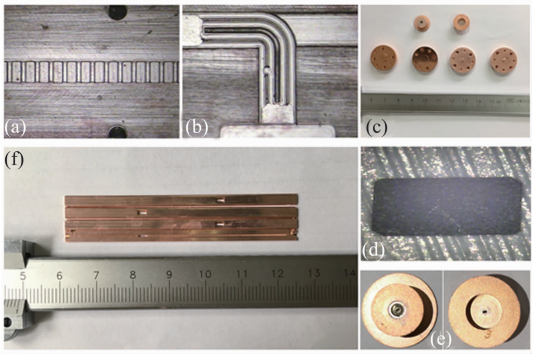


Fig. 14 The manufactured structure under the microscope (a) The main structure of the SWS, (b) Ridge-loaded input/output waveguide, (c) The flanges on both sides of the window, (d) The attenuator, (e) The components of pillbox window, (f) The overall framework of the structure
图 14 显微镜下的加工结构 (a) 慢波结构主要部分, (b) 脊加载输入输出波导, (c) 窗片两端的法兰盘, (d) 衰减器, (e) 盒型窗组件, (f) 结构整体框架

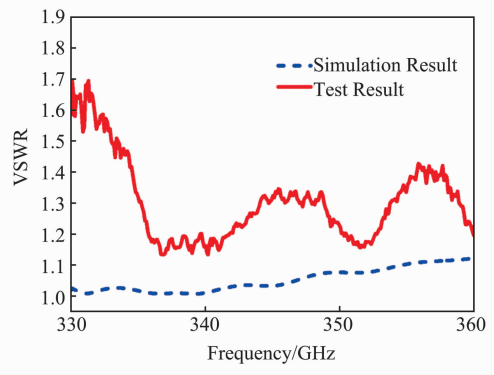


Fig. 15 The VSWR of the pillbox window compared with the simulated
图 15 盒型窗的电压驻波比测试结果与仿真结果的对比

The transmission coefficient of the pillbox window is given in Fig. 16 and the tested $S_{21}$ of the pillbox window is above −2.1 dB in the frequency range from 330 GHz to 360 GHz. The small discrepancy between two results is mainly caused by the accumulative effect of some deviations in the processing.

Next is the experiment of the whole high frequency system with input/output window. As shown in Fig. 17, the tested result of VSWR is below 2 in the frequency range from 335 GHz to 344 GHz. And it is match well with the simulation result while there is a little deviation between these. The reasons for this case mainly include the following points: the reflections caused by the inexact assembly of the structure, and the reflection introduced by the pillbox window.

## 4 Conclusions

In this paper, a filleted staggered double vane TWT

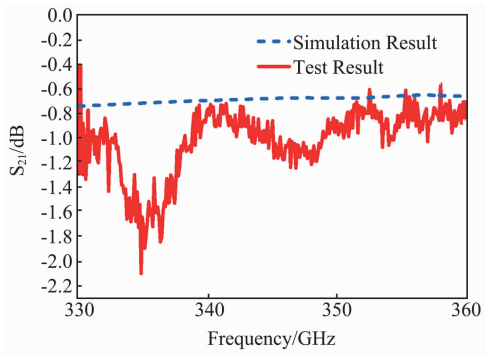


Fig. 16　The transmission coefficient of the pillbox window compared with the simulation results
图 16　盒型窗的传输系数测试结果与仿真结果的对比

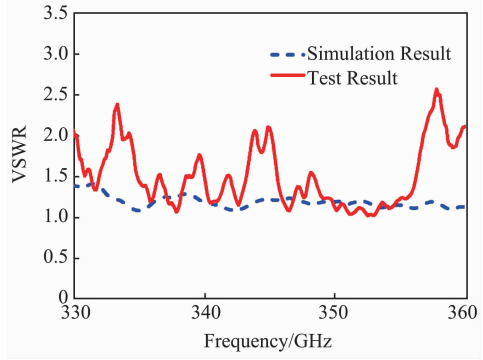


Fig. 17　The VSWR of the high frequency system with windows compared with the simulation result
图 17　包含盒型窗的高频系统的电压驻波比测试结果与仿真结果的对比

considered corrected conductivity has been obtained. The PIC simulation results indicate that the tube can obtain over 5 W output power range from 320 ~ 342 GHz, with beam voltage of 22.1 kV, beam current of 43 mA and 10 mW input signal. And an obvious improvement of output power with more than 28% in the operating wave band is obtained with phase-velocity taper. The experiment of the manufactured prototype consisted of slow wave structure, pillbox window and attenuator is carried out. The tested $S_{21}$ of the pillbox window is above −2.1 dB in the frequency range from 330 ~ 360 GHz and VSWR is below 1.35 in the frequency range from 334 ~ 355 GHz. And the tested VSWR of the high frequency system including the pillbox window is below 2 in the frequency range from 335 ~ 344 GHz.

## References


[1] Qiu J X, Levush B, Pasour J, *et al*. Vacuum tube amplifiers [J]. *IEEE Microwave Magazine*, 2009, **10**(7): 38 − 51.

[2] Kleine-Ostmann T, Jastrow C, Baaske K, *et al*. Field exposure and dosimetry in the THz frequency range [J]. *IEEE Transactions on Terahertz Science and Technology*, 2014, **4**(1): 12 − 25.

[3] Booske J H, Dobbs R J, Joye C D, *et al*. Vacuum electronic high power terahertz sources [J]. *IEEE Transactions on Terahertz Science and Technology*, 2011, **1**(1): 54 − 75.

[4] Sumathy M, Vinoy K J, Datta S K. Analysis of ridge-loaded folded-waveguide slow-wave structures for broadband traveling-wave tubes [J]. *IEEE Transactions on Electron Devices*, 2010, **57**(6): 1440 − 1446.

[5] Liang H T, Ruan C J, Xue Q Z, *et al*. An extended theoretical method used for design of sheet beam electron gun [J]. *IEEE Transactions on Electron Devices*, 2016, **63**(11): 4484 − 4492.

[6] Booske J H, Kumbasar A H, and Basten M A. Periodic focusing and ponderomotive stabilization of sheet electron beams [J]. *Physical Review Letters*, 1993, **71**(24): 3979 − 3982.

[7] Kyhl R L, Webster H F. Breakup of hollow cylindrical electron beams [J]. *IRE Transactions on Electron Devices*, 1956, **3**(4): 172 − 183.

[8] Shi X, Wang Z, Tang T, *et al*. Theoretical and experimental research on a novel small tunable PCM system in staggered double vane TWT [J]. *IEEE Transactions on Electron Devices*, 2015, **62**(12): 4258 − 4264.

[9] Shin Y M and Barnett L R. Intense wideband terahertz amplification using phase shifted periodic electron-plasmon coupling [J]. *Applied Physics Letters*, 2008, **92**(9): 091501.

[10] Shin Y M, Baig A, Barnett L R, *et al*. System design analysis of a 0.22 THz sheet-beam traveling-wave tube amplifier [J]. *IEEE Transactions on Electron Devices*, 2012, **59**(1): 234 − 240.

[11] Shin Y M, Barnett L R, and Luhmann N C. Strongly confined plasmonic wave propagation through an ultrawideband staggered double grating waveguide [J]. *Applied Physics Letters*, 2008, **93**(22): 221504.

[12] Shin Y M, Barnett L R, Luhmann N C. Phase-shifted traveling-wave-tube circuit for ultrawideband high-power submillimeter-wave generation [J]. *IEEE Transactions on Electron Devices*, 2009, **56**(5): 706 − 712.

[13] Shin Y M, Zhao J F, Barnett L R, *et al*. Investigation of terahertz sheet beam traveling wave tube amplifier with nanocomposite cathode [J]. *Physics of Plasmas*, 2010, **17**(12): 123105.

[14] Lai J Q, Gong Y B, Xu X, *et al*. W-band 1 kW staggered double-vane traveling-wave tube [J]. *IEEE Transactions on Electron Devices*, 2012, **59**(2): 496 − 503.

[15] Palm A, Sirigiri J, Shin Y M. Enhanced traveling wave amplification of co-planar slow wave structure by extended phase-matching [J]. *Physics of Plasmas*, 2015, **22**(9): 093121.

[16] Shi X, Billa L R, Gong Y, *et al*. High efficiency and high power staggered double vane TWT amplifier enhanced by velocity-taper design [J]. *Progress in Electromagnetics Research C*, 2016, **66**(5): 39 − 46.

[17] Gilmour A S. Principles of traveling-wave tubes [M]. Boston, MA: Artech House, 1994.

[18] Hammerstad E, Jensen O. Accurate models for microstrip computer-aided design [C]. 1980 *IEEE MTT-S International Microwave symposium Digest*, 1980: 407 − 409.

[19] Yang B B, Kirley M P, Booske J H. Theoretical and empirical evaluation of surface roughness effects on conductivity in the terahertz regime [J]. *IEEE Transactions on Terahertz Science and Technology*, 2014, **4**(3): 368 − 375.

[20] CST PS Tutorials, CST Corp., Houston, TX, USA, 2009. [Online]. Available: http://www.cst-china.cn/CST2009/product/